atoms

MDPI

Article

Structure and Bonding Patterns in C_5H_4 Isomers: Pyramidane, Planar Tetracoordinate Carbon, and Spiro Molecules

Sayon Satpati [1], Tarun Roy [1], Sandip Giri [2], Anakuthil Anoop [2], Venkatesan S. Thimmakondu [3] and Subhas Ghosal [1,*]

[1] Department of Chemistry, National Institute of Technology Durgapur, M G Avenue, Durgapur 713209, West Bengal, India
[2] Department of Chemistry, Indian Institute of Technology Kharagpur, Kharagpur 721302, West Bengal, India
[3] Department of Chemistry and Biochemistry, San Diego State University, San Diego, CA 92182-1030, USA
* Correspondence: subhas.ghosal@ch.nitdgp.ac.in

Simple Summary: Tetra-coordinated carbon-containing molecules generally form tetrahedral carbon geometries. However, there are continuous searches for other possible geometries of tetra-coordinated carbon which are non-classical in nature. However, planar tetra-coordinated carbon (ptC), where all four bonds of the carbon atom are in the same plane or the pyramidane structure in which tetra-coordinated carbon with all four bonds are on the same side of a plane, are good examples of non-classical structures. However, synthesis and experimental realization of these molecules are very challenging in the laboratory. In this paper, we have theoretically investigated nine unusual isomers of the molecular formula C_5H_4 and studied their stability and novel bonding patterns. One of the ptC compounds has been found to be thermodynamically more stable compared to its tetrahedral counterpart with a high value of dipole moment (μ = 4.64 D), which may be helpful for experimental detection in the laboratory or in the low-temperature regions of the interstellar medium.

Abstract: We have theoretically investigated nine unusual isomers of the molecular formula C_5H_4 using coupled cluster (CC) and density functional theory (DFT) methods. These molecules possess non-classical structures consisting of two pyramidanes, three planar tetracoordinate carbon (**ptC**), and four spiro types of isomers. Both the pyramidanes (tetracyclo-[2.1.0.$0^{1,3}$.$0^{2,5}$]pentane; **py-1** and tricyclo-[2.1.0.$0^{2,5}$]pentan-3-ylidene; **py-2**) are minima on the potential energy surface (PES) of C_5H_4. Among the three isomers containing ptC, (SP4)-spiro [2.2]pent-1-yne (**ptC-2**) is a minimum, whereas isomer, (SP4)-spiro [2.2]pent-1,4-diene (**ptC-1**) is a fourth-order saddle point, and (SP4)-sprio[2.2]pent-1,4-diylidene (**ptC-3**) is a transition state. The corresponding spiro isomers spiro[2.2]pent-1,4-diene (**spiro-1**), sprio[2.2]pent-1,4-diylidene (**spiro-3**) and spiro[2.2]pent-4-en-1-ylidene (**spiro-4**) are local minima, except spiro[2.2]pent-1-yne (**spiro-2**), which is a second-order saddle point. All relative energies are calculated with respect to the global minimum (pent-1,3-diyne; **1**) at the CCSD(T)/cc-pVTZ level of theory. Quantum chemical calculations have been performed to analyze the bonding and topological configurations for all these nine isomers at the B3LYP/6-311+G(d,p) level of theory for a better understanding of their corresponding electronic structures. **ptC-2** was found to be thermodynamically more stable than its corresponding spiro counterpart (**spiro-2**) and possesses a high dipole moment (μ = 4.64 D). The stability of the **ptC** structures with their higher spin states has been discussed.

Keywords: C_5H_4; DFT; coupled cluster; pyramidane; ptC; spiro

Citation: Satpati, S.; Roy, T.; Giri, S.; Anoop, A.; Thimmakondu, V.S.; Ghosal, S. Structure and Bonding Patterns in C_5H_4 Isomers: Pyramidane, Planar Tetracoordinate Carbon, and Spiro Molecules. *Atoms* **2023**, *11*, 96. https://doi.org/10.3390/atoms11060096

Academic Editor: Yew Kam Ho

Received: 30 April 2023
Revised: 6 June 2023
Accepted: 7 June 2023
Published: 10 June 2023

1. Introduction

Tetrahedral carbon is the fundamental paradigm of organic chemistry introduced independently by van't Hoff and Le-Bel in 1874 [1,2]. However, with the development of different experimental and theoretical margins, scientists have widely explored the

possibility of non-classical proclivities (i.e., anti-van't Hoff and Le Bel molecules) with unusual bonding features of the tetracoordinate carbon or silicon atoms [3–6]. Planar tetra-coordinated carbon (ptC), where all four bonds of the carbon atom are in the same plane or the pyramidane structure in which tetra-coordinated carbon with all four bonds are on the same side of a plane, are good examples of non-classical structures. Along with these structures, spiro compounds with tetrahedral carbon centers have also become esoteric targets for organic chemists to design and synthesize in the laboratory [7–10].

Although simple hydrocarbons with ptC moiety have not been experimentally detected in the laboratory to date, many theoretical and experimental research groups have designed such molecules [4,5,9–17]. Hoffmann et al. explored the stability of planar methane and its derivatives for the first time in 1970 [18]. Based on their calculations, they have suggested a few rules to stabilize molecules with ptC, such as to include the lone pair in the bonding framework by replacing one or more hydrogen atoms with good σ-donor/π-acceptor ligands or, alternatively, by incorporating the lone pair into a (4n + 2) π delocalized system. Commonly, two approaches have been used to design ptC structures: the first is to obtain the planar structure under forcible structural constraints from supporting fragments [19–21], and the second is through electronic stabilization of the ptC center using σ-donor and π-accepting groups by employing transition metal fragments or main group elements and controlling suitable charge on the skeleton [14,17,19,21–32]. Rasmussen and Radom discussed the evolution of the potential solution of this problem by considering ptC in the cycloalkane systems [33].

Despite being challenging, molecules with a ptC atom among hydrocarbons have been drawing huge attention from theoretical scientists. Sastry et al. theoretically designed several neutral hydrocarbons with ptCs and discussed the stabilization of the planar arrangements through the negative of the absolute shielding nucleus independent chemical shift (NICS) values and suggested the unique bonding mode of the planar arrangements, which is stabilized through high delocalization of π –framework or aromatization of the rings [34]. Thimmakondu et al. have theoretically shown that two isomers of C_5H_2 with ptC atom, (SP-4)-spiro[2.2]pent-1,4-dien-1,4-diyl and (SP-4)-spiro[2.2]pent-1,4-dien-1,5-diyl [35] that can act as reactive intermediates for the formation of ethynylcyclopropenylidene, which had been astronomically identified in Taurus Molecular Cloud-1 (TMC-1) [36,37] as well as in the laboratory [38–40]. The Vennapusa group has recently considered the semi-saturated planar tetracoordinate carbon molecule of C_7H_4 molecular formula and studied the nonadiabatic relaxation dynamics [41]. Priyakumar et al. have studied the stereomutation between [*R*]- and [*S*]-stereoisomers of tetrahedral centers via the planar tetracoordinate atoms [42].

Apart from ptCs, pyramidane structures have also shown unusual bonding patterns. In chemistry, the compound possessing the shape of a square pyramid is called pyramidane. Four bonds are symmetrically oriented around a central axis when the pyramidal carbon lies on a C_{4v} axis. Stohrer and Hoffman had first introduced the stable pyramidal structure for $(CH)_5^+$ in 1972 followed by several other groups over the years [43–45]. Schaefer et al. explored the potential energy surface of the molecular formula of C_5H_4 around the pyramidane isomers [46]. Errol Lewars theoretically studied the pyramidane, tetracyclo[2.1.0.$0^{1,3}0^{2,5}$]pentane, a neutral minima isomer in the potential energy surface of C_5H_4 at the QCISD(T)/6-31G*//MP2(FC)/6-31G* level of theory [47]. Besides the pyramidane in hydrocarbons, few silicon analogues of similar structures have been studied theoretically where stable pyramidal structures had been reported with the bare apical silicon atoms [48–50].

A comprehensive knowledge of the electronic structures of these hydrocarbons can provide valuable insights into the principles of non-classical bonding and can have practical implications in designing new materials with specific electronic properties. In this paper, we endeavor to the electronic structures of the possible ptC, pyrimidine, and spiro type of isomers of the molecular formula C_5H_4 using density functional theory (DFT) and coupled cluster (CC) methods. C_5H_4 is one of the simplest structures where all these stereochemical

proclivities are possible. Considering the different types of unusual bonding patterns in the non-classical molecules, nine hydrocarbons with molecular formula C_5H_4 have been considered for the present study. Among the nine isomers, two pyramidane structures are tetracyclo-[2.1.0.0^{1,3}.0^{2,5}]pentane (**py-1)** and tricyclo-[2.1.0.0^{2,5}]pentan-3-ylidene (**py-2**); three ptCs are (SP4)-spiro[2.2]pent-1,4-diene (**ptC-1**), (SP4)-sprio[2.2]pent-1-yne (**ptC-2**), (SP4)-sprio[2.2]pent-1,4-diylidene (**ptC-3**); and rest of the four isomers are spiro compounds: spiro[2.2]pent-1,4-diene (**spiro-1**), spiro[2.2]pent-1-yne (**spiro-2**), sprio[2.2]pent-1,4-diylidene (**spiro-3**), and spiro[2.2]pent-4-en-1-ylidene (**spiro-4**). Different bonding topologies have been discussed to get an insight of the non-classical nature of these molecules and to explain the bonding patterns of these isomers. Among the three ptCs, the **ptC-2** is the only isomer which is at a minimum on the C_5H_4 PES and more stable than the corresponding tetrahedral form (**spiro-2**). The kinetic stability of these non-classical structures has been also studied using ab initio molecular dynamics (AIMD) simulations.

2. Computational Methodology

Initially, we designed 13 possible geometries of molecular formula C_5H_4 consisting of three pyramidanes, five ptCs, and five spiro molecules (Figure S1). These structures were subjected to geometry optimization using DFT at the B3LYP [51,52] /6-311+G(d,p) [53,54] level of theory without applying any geometrical or symmetry constraints. Some initial structures did not converge to the desired geometry; however, after multiple trials we could optimize two pyramidanes, three ptCs, and four spiro structures. These optimized structures were then subjected to frequency calculation to check the number of imaginary frequencies (NImag) and to ascertain whether the isomer is a minimum or higher-order saddle point or transition state on the C_5H_4 PES.

Furthermore, the structures of all nine isomers have been optimized and frequencies have been calculated using the Møller–Plesset perturbation theory (MP2) [55] and also at the ωB97XD [56,57] /6-311+G(d,p) level that incorporates the empirical dispersion corrections [56]. Further, considering the DFT-optimized geometries as initial guess structures, geometry optimization has been carried out at the coupled-cluster singles and doubles with quasi-perturbative triple excitation [CCSD(T)] methods [58–60] using Dunning's correlation-consistent polarized valence triple-zeta basis set (cc-pVTZ) [61–63] for all isomers. After geometry optimization, harmonic vibrational frequencies were computed at the fc-CCSD(T)/cc-pVTZ level of theory. NICS calculations have been carried out to evaluate the aromatic nature of molecules at the B3LYP/6-311+G(d,p) level. All DFT calculations were performed using the Gaussian 09 suite of programs [64] and all CC calculations have been carried out using CFOUR program package [65] and ORCA [66]. The nature of bonding between the C-C and C-H atoms have been studied using the topological analysis of 'atoms in molecule' (AIM) formalism employing the multifunctional wavefunction analyzer program, Multiwfn [67]. AIMD simulation calculations have been performed to check the kinetic stability of these isomers under different thermal conditions [68].

3. Results and Discussions

All nine isomers considered in the present study are shown in Figure 1 and 3D ball-stick models of the optimized geometries, along with the atom numbers, of all the isomers are shown in Figure 2. The relative energies of these isomers are calculated with respect to the most stable isomer, pent-1,3-diyne (**1**), which is the global minimum on the C_5H_4 PES. Here we note that, **1** had been detected in the dark dust cloud of TMC-1 and in the interstellar medium (ISM) back in 1984 [69,70]. The detection of this molecule in astrophysical environments highlights its importance and motivates the current study. Later, in 2017, M. Araki et al. identified the same molecule in the low-mass star-forming region L1527 [71]. Very recently, J. Cernicharo et al. identified the deuterated species of global minima (CH_2DC4H) in TMC-1 with the help of the QUIJOTE line survey [72], which underscores the relevance of investigating the electronic structures of these hydrocarbons in the context of astrophysical chemistry.

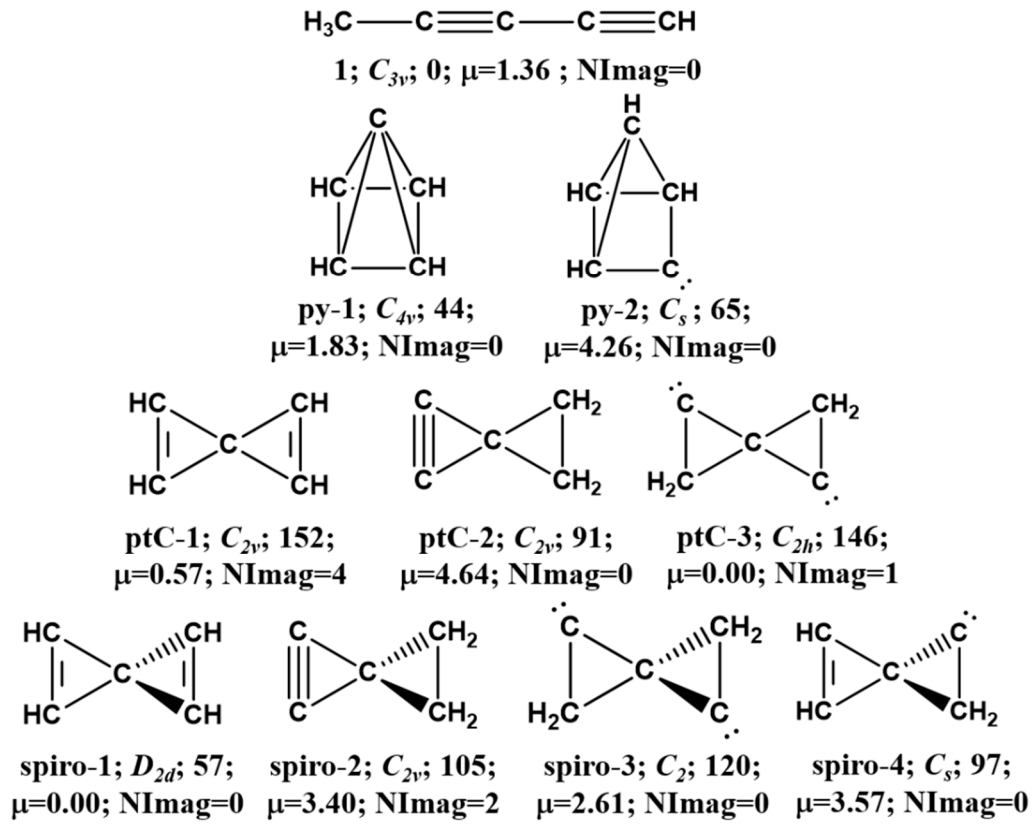

Figure 1. Electronic structure of nine unusual high energy isomers of molecular formula C_5H_4. Point group symmetry, ZPVE-corrected relative energies (in kcal mol^{-1}), absolute dipole moment values (in Debye) and number of imaginary frequencies (NImag) are calculated at the fc-CCSD(T)/cc-pVTZ level of theory.

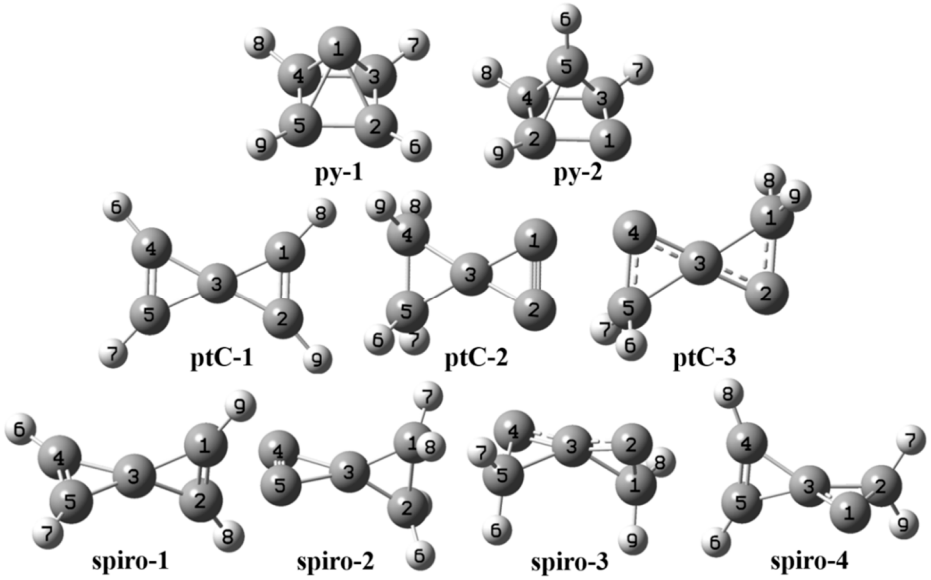

Figure 2. 3D ball-stick models of the same molecules along with the atom numbers are shown in Figure 1.

In Table 1, we present the zero-point vibrational energy (ZPVE) corrected relative energies (ΔE_0; in kcal mol^{-1}), point group symmetry, numbers of imaginary frequencies (NImag), and the total dipole moment (μ; in Debye) at various levels of theory for all the isomers. However, we have considered the relative energy values calculated at the

fc-CCSD(T)/cc-pVTZ level of theory in all our further discussion as they are much more accurate and reliable than the DFT method employed here. The Wiberg bond indices (WBIs) for the different C-C bonds in each isomer, obtained from natural bond orbital (NBO) analysis, are calculated at the ωB97XD/6-311+G(d,p) level and listed in Table 2. These WBIs serve as indicators of the relative bond strengths between carbon atoms in the respective isomers.

Table 1. ZPVE-corrected relative energies (ΔE_0; in kcal mol^{-1}), points groups, numbers of imaginary frequencies, and the total dipole moments (μ; in Debye) of the isomers of molecular formula C_5H_4 calculated at different levels of theory.

Molecule	Point-Group	B3LYP/6-311+G(d,p)	ωB97XD/6-311+G(d,p)	MP2/6-311+G(d,p)	fc-CCSD(T)/cc-pVTZ	NImag	Dipole Moment
Pent-1,3-diyne	C_{3v}	0	0	0	0	0	1.36
py-1	C_{4v}	55	42	43	44	0	1.83
py-2	C_s	75	61	66	65	0	4.26
ptC-1	C_{2v}	143	140	146	152	4	0.57
ptC-2	C_{2v}	92	85	93	91	0	4.64
ptC-3	C_{2h}	142	139	150	146	1	0
spiro-1	D_{2d}	59	52	59	57	0	0
spiro-2	C_{2v}	108	102	109	105	2	3.40
spiro-3	C_2	120	117	128	120	0	2.61
spiro-4	C_s	97	90	102	97	0	3.57

Table 2. WBI indices for all nine isomers calculated at ωB97XD/6-311+G(d,p) level of theory.

py-1		**py-2**		**ptC-1**		**ptC-2**		**ptC-3**		**spiro-1**		**spiro-2**		**spiro-3**		**spiro-4**	
C1-C2	0.70	C1-C2	1.07	C1-C2	1.67	C1-C2	1.56	C1-C2	1.12	C1-C2	1.88	C1-C2	0.96	C1-C2	1.06	C1-C2	0.96
C1-C3	0.70	C1-C3	1.07	C1-C3	0.98	C1-C3	1.13	C1-C3	0.72	C1-C3	0.97	C1-C3	1.01	C1-C3	0.81	C1-C3	1.14
C1-C4	0.70	C2-C3	0.56	C2-C3	0.98	C2-C3	1.13	C2-C3	1.20	C2-C3	0.97	C2-C3	1.01	C2-C3	1.13	C2-C3	1.01
C1-C5	0.70	C3-C4	0.80	C3-C4	0.98	C3-C4	0.87	C3-C4	1.20	C3-C4	0.97	C3-C4	0.97	C3-C4	1.13	C3-C4	0.87
C2-C3	1.10	C3-C5	0.80	C3-C5	0.98	C3-C5	0.87	C3-C5	0.72	C3-C5	0.97	C3-C5	0.97	C3-C5	1.06	C3-C5	0.87
C3-C4	1.10	C4-C5	0.84	C4-C5	1.67	C4-C5	1.02	C4-C5	1.12	C4-C5	1.88	C4-C5	2.44	C4-C5	1.06	C4-C5	1.99
C4-C5	1.10	C4-H8	1.03	C1-H8	0.88	C4-H8	0.91	C1-H8	0.90	C1-H9	0.90	C1-H7	0.90	C1-H8	0.90	C2-H7	0.91
C5-C2	1.10	C4-H9	1.03	C2-H9	0.88	C4-H9	0.91	C1-H9	0.90	C2-H8	0.90	C1-H8	0.90	C1-H9	0.90	C2-H9	0.91
C2-H6	0.91	C5-H6	0.91	C4-H6	0.88	C5-H6	0.91	C5-H6	0.90	C4-H6	0.90	C2-H6	0.90	C5-H6	0.90	C4-H8	0.90
C3-H7	0.91	C5-H7	0.91	C5-H7	0.88	C5-H7	0.91	C5-H7	0.90	C5-H7	0.90	C2-H9	0.90	C5-H7	0.90	C5-H6	0.90
C4-H8	0.91	C1-C2	0.90														
C5-H9	0.91	C1-C3	0.89														

The electronic distribution in the frontier molecular orbitals is analyzed by examining the highest occupied molecular orbital (HOMO) and the lowest unoccupied molecular orbital (LUMO) for each isomer calculated at the ωB97XD/6-311+G(d,p) level, which are depicted in Figure 3. Here we note that, as reported earlier, the B3LYP functional without dispersion correction may not be able to reproduce accurate orbital energies for the simple hydrocarbon molecules [73]. However, the results obtained using the B3LYP density functional have been included in the ESI for reference. The electron localization function (ELF) analysis is carried out to assess the extent of electron delocalization in the molecular systems at the same level of theory. Figure 4 presents the color-filled ELF plots of nine isomers being studied. The bond critical points (BCPs) and ring critical points (RCPs) calculated at the ωB97XD/6-311+G(d,p) level of theory are listed in Figure 5. Electron density descriptors (in a.u.) at the (3, –1) bond critical points (BCP) are calculated for all nine isomers along with the topological parameters such as Hamiltonian kinetic energy $K(r_c)$, electron density $\rho(r_c)$, Laplacian electron density $\nabla^2 \rho(r_c)$, Lagrangian kinetic energy $G(r_c)$, potential energy density $V(r_c)$, total energy density $E(r_c)$ or $H(r_c)$, ELF, $G(r_c)/V(r_c)$, and $G(r_c)/\rho(r_c)$ and listed in Table 3. The spectroscopic parameters such as inertial axis dipole moments along with their components, rotational constants and the centrifugal distortion constants, and the final optimized Cartesian coordinates are given in the Supporting Information.

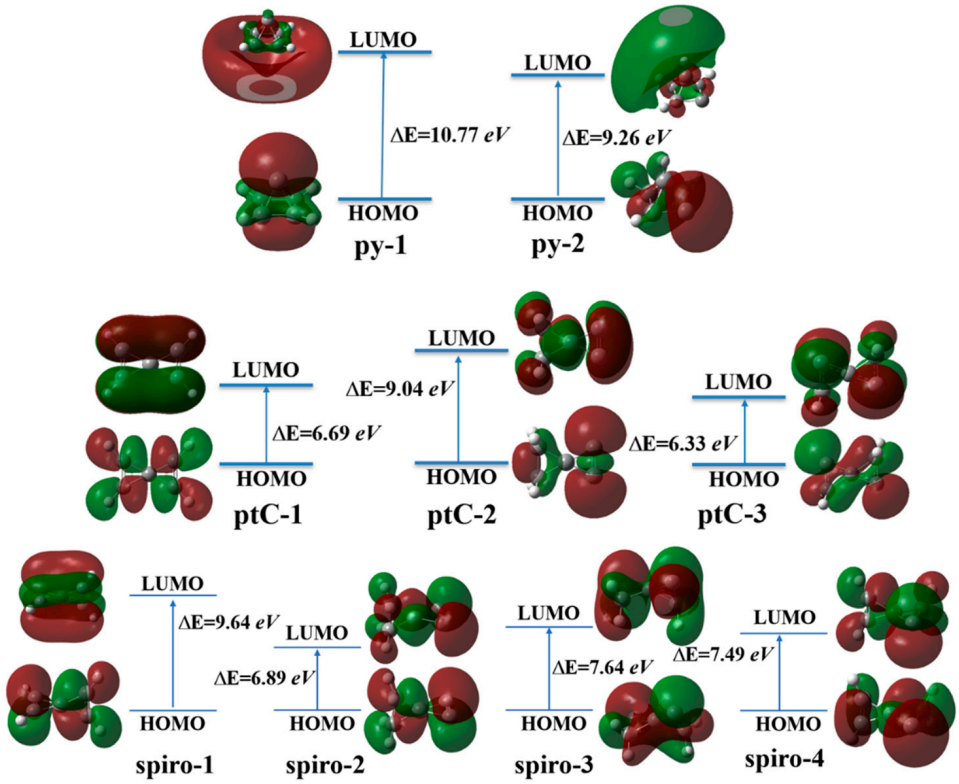

Figure 3. Molecular orbitals (HOMO and LUMO) and their energy gap of all nine isomers calculated at the ωB97XD/6-311+G(d,p) level of theory.

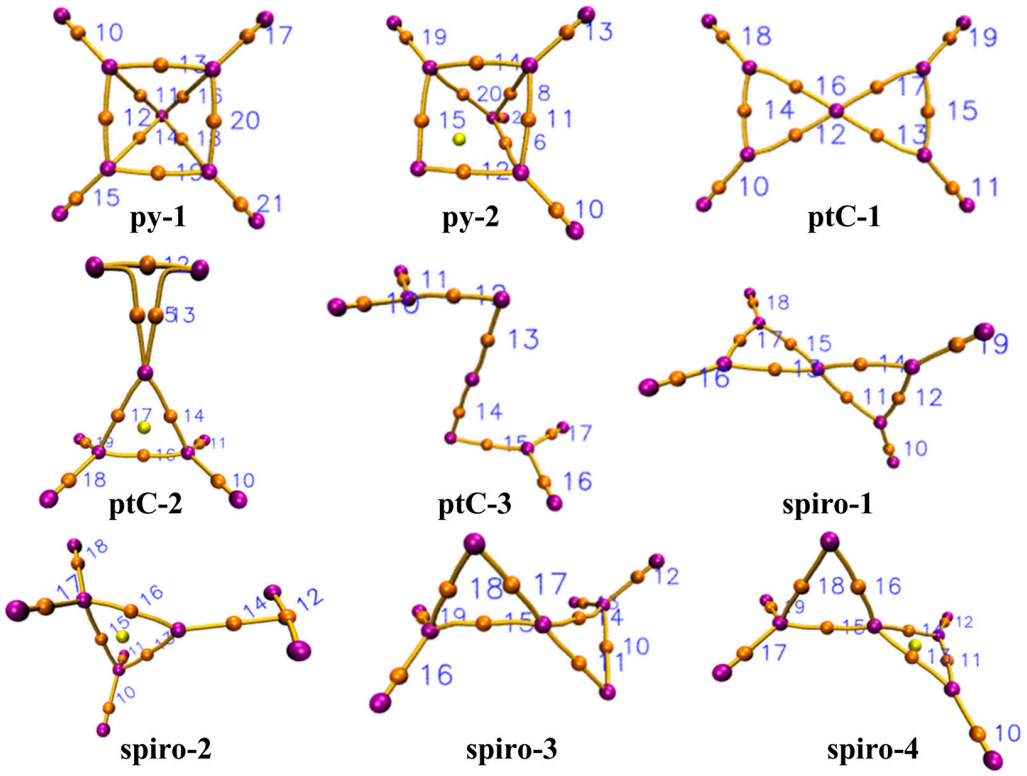

Figure 4. Molecular graph representation of the pyramidane, ptC and spiro isomers of C_5H_4. Atoms are shown in violet color, bond critical points in orange color, and ring critical points in yellow color calculated at the ωB97XD /6-311+G(d,p) level of theory.

Table 3. Electron density descriptors (in a.u.) at the (3, –1) bond critical points (BCP) obtained from the ωB97XD/6-311+G(d,p) level for all the nine isomers. The topological parameters such as Hamiltonian kinetic energy K(r_c), ρ(r_c), Laplacian electron density ($\nabla^2\rho(r_c)$), Lagrangian kinetic energy G(r_c), potential energy density V(r_c), energy density E(r_c) or H(r_c), ELF, G(r_c)/V(r_c), and G(r_c)/ρ(r_c) at the critical points are also given.

Molecules	BCP	Index	$K(r_c)$	$\rho(r_c)$	$(\nabla^2\rho(r_c))$	$G(r_c)$	$V(r_c)$	$H(r_c)$	ELF	$G(r_c)/V(r_c)$	$G(r_c)/\rho(r_c)$
py-1	8(H)--4(C)	10	0.284	0.285	−1.002	0.034	−0.318	−0.284	0.991	−0.106	0.119
	4(C)--1(C)	11	0.106	0.169	−0.021	0.100	−0.206	−0.106	0.685	−0.487	0.595
	4(C)--3(C)	12	0.257	0.274	−0.631	0.099	−0.356	−0.257	0.918	−0.278	0.361
py-2	9(H)--2(C)	10	0.282	0.283	−0.992	0.034	−0.316	−0.282	0.991	−0.107	0.119
	2(C)--4(C)	11	0.220	0.253	−0.507	0.094	−0.314	−0.220	0.905	−0.298	0.371
	2(C)--1(C)	12	0.233	0.256	−0.560	0.093	−0.326	−0.233	0.910	−0.285	0.364
ptC-1	7(H)--5(C)	10	0.255	0.266	−0.876	0.036	−0.290	−0.255	0.987	−0.123	0.134
	5(C)--3(C)	12	0.177	0.225	−0.245	0.116	−0.292	−0.177	0.811	−0.395	0.513
	5(C)--4(C)	14	0.364	0.327	−0.899	0.140	−0.504	−0.364	0.910	−0.277	0.427
ptC-2	6(H)--5(C)	10	0.278	0.280	−0.960	0.038	−0.315	−0.278	0.988	−0.119	0.134
	2(C)--1(C)	12	0.434	0.358	−1.118	0.154	−0.588	−0.434	0.919	−0.262	0.430
	2(C)--3(C)	13	0.161	0.231	0.091	0.183	−0.344	−0.161	0.649	−0.533	0.795
	5(C)--3(C)	14	0.189	0.230	−0.375	0.096	−0.285	−0.189	0.872	−0.335	0.414
	5(C)--4(C)	16	0.218	0.251	−0.513	0.089	−0.307	−0.218	0.911	−0.291	0.356
ptC-3	6(H)--5(C)	10	0.274	0.278	−0.948	0.037	−0.310	−0.274	0.989	−0.118	0.132
	5(C)--4(C)	12	0.278	0.284	−0.695	0.104	−0.381	−0.278	0.920	−0.272	0.365
	4(C)--3(C)	13	0.237	0.250	−0.426	0.131	−0.368	−0.237	0.827	−0.355	0.522
spiro-1	8(H)--2(C)	10	0.274	0.277	−0.953	0.036	−0.310	−0.274	0.989	−0.116	0.130
	2(C)--3(C)	11	0.203	0.243	−0.378	0.109	−0.312	−0.203	0.862	−0.348	0.447
	2(C)--1(C)	12	0.403	0.341	−0.909	0.176	−0.578	−0.403	0.881	−0.304	0.515
spiro-2	9(H)--2(C)	10	0.272	0.276	−0.930	0.040	−0.312	−0.272	0.986	−0.128	0.144
	4(C)--5(C)	12	0.599	0.423	−1.476	0.230	−0.829	−0.599	0.898	−0.277	0.544
	2(C)--3(C)	13	0.243	0.266	−0.583	0.098	−0.341	−0.243	0.913	−0.286	0.367
	2(C)--1(C)	15	0.171	0.222	−0.334	0.087	−0.258	−0.171	0.878	−0.338	0.392
spiro-3	2(C)--1(C)	10	0.233	0.259	−0.522	0.103	−0.336	−0.233	0.897	−0.306	0.396
	2(C)--3(C)	11	0.277	0.274	−0.578	0.132	−0.409	−0.277	0.862	−0.323	0.483
	1(C)--8(H)	12	0.270	0.276	−0.934	0.037	−0.307	−0.270	0.988	−0.120	0.134
	3(C)--1(C)	14	0.160	0.216	−0.157	0.121	−0.282	−0.160	0.772	0.430	0.561
spiro-4	8(H)--4(C)	10	0.282	0.282	−0.997	0.033	−0.315	−0.282	0.991	−0.104	0.116
	4(C)--5(C)	11	0.454	0.362	−1.017	0.200	−0.654	−0.454	0.874	−0.306	0.553
	4(C)--3(C)	13	0.170	0.221	−0.236	0.111	−0.281	−0.170	0.814	−0.395	0.502
	3(C)--2(C)	15	0.219	0.252	−0.463	0.103	−0.322	−0.219	0.886	−0.320	0.411
	3(C)--1(C)	16	0.294	0.295	−0.735	0.111	−0.405	−0.294	0.920	−0.273	0.375

The detailed structural studies of these nine unusual C_5H_4 isomers are discussed in the following sub-sections.

3.1. Pyramidane

The simplest possible hydrocarbon molecule with one pyramidal C atom can be represented by isomers tetracyclo-[2.1.0.$0^{1,3}$.$0^{2,5}$]pentane (**py-1**) and tricyclo-[2.1.0.$0^{2,5}$]pentan-3-ylidene (**py-2**) (Figure 1). These molecules pose inverted tetrahedral geometry (so-called "umbrella") configurations of the tetra-coordinated C atom. Although a fascinating target for synthetic chemists, to the best of our knowledge, no pyramidane hydrocarbon molecule and its structural isomers has been isolated as a stable compound to date. Both the pyramidane structures (**py-1** and **py-2**) are minima on the C_5H_4 PES, having no imaginary frequency at the fc-CCSD(T)/cc-pVTZ level of theory. **py-1** and **py-2** are found to be 44 and 65 kcal mol^{-1} higher in energy than the global minima **1**, respectively.

In **py-1,** one carbon atom is on top of the pyramid, which is attached to the base with the four carbon atoms in a cyclobutene ring. The ground electronic state of **py-1** is $^1A_1$ (C_{4v} symmetry) with the electronic configuration $(1a_1)^2(1e)^4(1b_2)^2(2a_1)^2(3a_1)^2(2e)^4(4a_1)^2(5a_1)^2(2b_2)^2(1b_1)^2(3e)^4(4e)^4(6a_1)^2$. From the electronic configuration, it is clear that the overall stabilization of **py-1** is due to the formation of two doubly degenerated frontier occupied molecular orbitals, HOMO-1 (4e) and HOMO-2 (3e); the HOMO ($6a_1$) possess a lone pair

of electrons (Figure 3). This is due to the strong overlap between the π-orbital of the cyclobutadiene ring and the apical carbon p_x, p_y, and p_z orbitals. This observation is also supported by the high energy gap between the HOMO-LUMO ($\Delta E_{HOMO\text{-}LUMO}$ = 10.77 eV) of **py-1** at the ground (singlet) electronic state compared to other isomers. Based on the WBIs (Table 2), it can be inferred C_{apical}-C_{basal} (bond order 0.70) is weaker than C_{basal}-C_{basal} (bond order 1.10) and C_{basal}-H (bond order 0.91). There is a possibility of formation of an aromatic $C_4H_4^{2-}$ ring (cycobutadienyl dianion) in the base with a capping C^{2+} moiety; however, this aspect has not been considered in the present study.

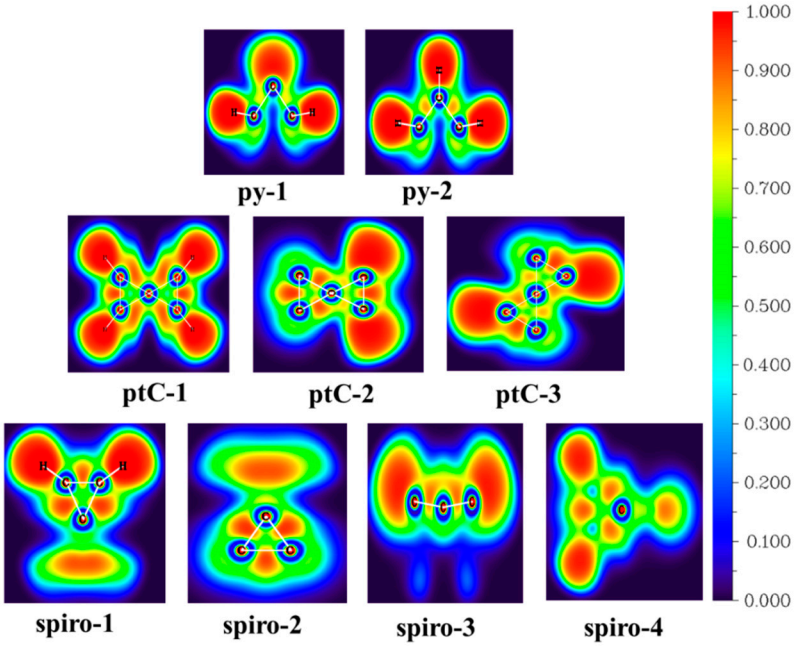

Figure 5. Color-filled electron localization function (ELF) plots of all nine isomers calculated at the ωB97XD/6-311+G(d,p) level of theory.

In the case of the **py-2**, the top carbon atom is attached to one hydrogen atom and the base consists of a four-membered ring containing three -CH groups and one carbene carbon. The ground electronic state of **py-2** is $^1A'$ (C_s symmetry) with electronic configuration (1-3a′)^2(1a′′)^2(4-5a′)^2(2a′′)^2(6-10a′)^2(3-4a′′)^2(11a′)^2(5a′′)^2(12a′)^2. The observed HOMO-LUMO energy gap for **py-2** is also high ($\Delta E_{HOMO\text{-}LUMO}$ = 9.26 eV). The WBI value for **py-2** of C_{apical}-$C_{basal(attached\ to\ hydrogen)}$ is 0.81, whereas C_{apical}-$C_{basal(carbene\ carbon)}$ is 0.59 which implies more electrostatic interaction between the apical carbon and the basal carbene carbon. Again, the WBI value for C_{basal}-C_{basal} bond is 1.06, which indicates a possible single-bond character.

3.2. Planar Tetracoordinate Carbon (ptC)

The (SP4)-spiro[2.2]pent-1,4-diene (**ptC-1**) refers to the molecule where the central carbon atom is attached to four other carbon atoms in one plane. However, the hydrogen atoms attached to the four terminal carbon atoms are not in the same plane. Therefore, the point group symmetry for this molecule is C_{2v}. **ptC-1** is a fourth-order saddle point on the C_5H_4 PES having four imaginary frequencies. Here we note that if all four hydrogen atoms are forced to remain in the same plane of the carbon atoms, the molecule becomes a fifth-order saddle point with D_{2h} molecular symmetry. However, if we remove two electrons from the planar form, the dicationic form of the molecule becomes a minimum energy isomer on the C_5H_4 PES. The above phenomenon can be explained by looking into the electronic structure of both systems. The removal of the electron pair from the **ptC-1** leads to the delocalization of the electrons and the formation of two aromatic cyclopropenyl rings containing two electrons each.

The ground electronic state of **ptC-1** is $^1A_2$ with the electronic configuration $(1a_1)^2(1b_1)^2(2a_1)^2(1a_2)^2(1b_2)^2(3a_1)^2(2b_1)^2(4a_1)^2(2b_2)^2(2a_2)^2(3b_1)^2(5\text{-}6a_1)^2(3b_2)^2(4b_1)^2(3a_2)^2$. This isomer is 152 kcal mol^{-1} higher in energy compared to **1**. However, the HOMO-LUMO energy gap ($\Delta E_{HOMO\text{-}LUMO}$ = 6.69 eV) is relatively low. The WBI value of $C_{terminal}$-$C_{terminal}$ is 1.66, indicating double bonding character, whereas the WBI bond order for $C_{central}$-$C_{terminal}$ is 0.98, which signifies a C-C single bond.

The (SP4)-sprio[2.2]pent-1-yne (**ptC-2**) refers to the ptC moiety where one side of the ring is attached to two sp^3 hybridized carbon atoms and the other side is attached to two sp-hybridized carbon atoms (Figure 1). Therefore, all the four hydrogen atoms are attached to the side of the sp^3-hybridized carbon atoms. The point group symmetry for this molecule is C_{2v}. **ptC-2** is found to be the only planar tetracoordinate carbon which is a minimum on the C_5H_4 PES. It is 91 kcal mol^{-1} higher in energy compared to the global minimum. It is worth mentioning here that this isomer is 14 kcal mol^{-1} lower in energy compared to the corresponding tetrahedral form (**spiro-2**). However, **ptC-2** has a substantial HOMO-LUMO energy gap ($\Delta E_{HOMO\text{-}LUMO}$ = 9.04 eV) compared to **spiro-2** ($\Delta E_{HOMO\text{-}LUMO}$ = 6.89 eV). The dicationic form of **ptC-2** is also a planar tetracoordinate carbon and a minimum energy structure on the C_5H_4 PES.

The ground electronic state of **ptC-2** is $^1A_1$ with the electronic configuration $(1a_1)^2(2a_1)^2(1b_2)^2(3a_1)^2(2b_2)^2(4a_1)^2(5a_1)^2(3b_2)^2(6a_1)^2(1b_1)^2(4b_2)^2(7a_1)^2(1a_2)^2(8a_1)^2(2b_1)^2(5b_2)^2(9a_1)^2$. The WBI value of ptC-2 for $C_{central}$-$C_{terminal(no\ hydrogen)}$ is 1.13, $C_{central}$-$C_{terminal(attached\ hydrogen)}$ is 0.87 which indicates the stronger C-C between the central carbon atom and terminal carbon atoms having no hydrogen. Again, WBI value for $C_{terminal(attached\ hydrogen)}$-$C_{terminal\ (attached\ hydrogen)}$ is 1.02 indicating C-C single bond character. However, $C_{terminal(no\ hydrogen)}$-$C_{terminal(no\ hydrogen)}$ has WBI value of 1.56 which corresponds closely to a double bond instead of triple bond. This anomaly is also evident from the molecular graph representation (Figure 5), and the ELF value (0.66) between $C_{central}$-$C_{terminal(no\ hydrogen)}$ bond.

The (SP4)-sprio[2.2]pent-1,4-diylidene (**ptC-3**) refers to the molecule where one carbon is in the center attached to the four carbon atoms in the same plane. Among the four carbon atoms, two carbon atoms are carbene in nature and lie opposite to each other. The other two carbon atoms are sp^3-hybridized and have two hydrogen molecules attached to them. The point group symmetry for this molecule is C_{2h}. **ptC-3** is 146 kcal mol^{-1} higher in energy compared to the corresponding global minima. However, **ptC-3** is a transition state, having an imaginary frequency on the C_5H_4 PES. An intrinsic reaction coordinate (IRC) calculation reveals **ptC-3** connects the stereomutation of the **spiro-3** molecules at both ends of the reaction coordinates, as shown in Figure S1.

The ground electronic state of **ptC-3** is ^1B_u with the electronic configuration $(1a_g)^2(1b_u)^2(2a_g)^2(2b_u)^2(3a_g)^2(4a_g)^2(3b_u)^2(4b_u)^2(5a_g)^2(1a_u)^2(1b_g)^2(6a_g)^2(5b_u)^2(6b_u)^2(7a_g)^2(2a_u)^2(7b_u)^2$. The WBI value for $C_{central}$-$C_{terminal(no\ hydrogen)}$ = 1.23, $C_{central}$-$C_{terminal(attached\ hydrogen)}$ = 0.70, and $C_{terminal(no\ hydrogen)}$-$C_{terminal(attached\ hydrogen)}$ = 1.12 designates to the stronger C-C bond between the central carbon and the terminal carbon having no attached hydrogen.

3.3. Spiro

In the case of the spiro[2.2]pent-1,4-diene (**spiro-1**) molecule, the central carbon atom is attached to the four CH groups in a tetrahedral manner with the molecular symmetry of D_{2d}. The tetrahedral form (**spiro-1**) is a minimum on the PES of the molecular formula C_5H_4. **spiro-1** is 57 kcal mol^{-1} higher than **1**. Removing two electrons from **spiro-1** leads to the dicationic form of spiropentadiene at a higher-order saddle point. The delocalized rings of the dication of the spiropentadiene bring the aromatic character and explain the stability of the molecules. The ground electronic state of **spiro-1** is ^1E with the electronic configuration $(1a_1)^2(1b_2)^2(2a_1)^2(1e)^4(3a_1)^2(2b_2)^2(2e)^4(4a_1)^2(3b_2)^2(5a_1)^2(3e)^4(4b_2)^2(4e)^4$. This molecule possesses a higher HOMO-LUMO energy gap ($\Delta E_{HOMO\text{-}LUMO}$ = 9.64 eV) than the corresponding **ptC-1** ($\Delta E_{HOMO\text{-}LUMO}$ = 6.69 eV). The WBI value of **spiro-1** for $C_{terminal}$-

$C_{terminal}$ = 1.88 and $C_{central}$-$C_{terminal}$ = 0.97 indicates the double bond and single bond characters, respectively.

In the spiro[2.2]pent-1-yne (**spiro**-2) molecule, the central carbon atom is attached to the two -CH_2 groups and two sp-hybridized carbon atoms in a tetrahedral manner with the molecular symmetry of C_{2v}. The tetrahedral form (**spiro-2**) is not a minimum on the PES, as it corresponds to a second-order saddle point on C_5H_4 PES having two imaginary frequencies. The ground electronic state of this molecule is $^1B_2$ with the electronic configuration $(1a_1)^2(2a_1)^2(1b_2)^2(3a_1)^2(1b_1)^2(4a_1)^2(5a_1)^2(2b_2)^2(6a_1)^2(2b_1)^2(7a_1)^2(3b_1)^2(1a_2)^2(3b_2)^2(8a_1)^2(9a_1)^2(4b_2)^2$. The WBI value of spiro-2 for $C_{terminal(no\ attached\ hydrogen)}$-$C_{terminal(no\ attached\ hydrogen)}$ = 2.44, $C_{terminal(attached\ hydrogen)}$-$C_{terminal(attached\ hydrogen)}$ = 0.96, $C_{central}$-$C_{terminal(no\ attached\ hydrogen)}$ = 0.97, and $C_{central}$-$C_{terminal(attached\ hydrogen)}$ =1.01 indicates triple bond, single bond, single bond and single bond characters, respectively.

In spiro[2.2]pent-1,4-diylidene (**spiro-3**), the central carbon atom is attached to the two carbene carbon, forming the allene-type molecules in a tetrahedral manner with the molecular symmetry of C_2 and a minimum energy isomer in C_5H_4 PES. The ground electronic state of **spiro-3** is ^1B with the electronic configuration $(1a)^2(1b)^2(2a)^2(2b)^2(3a)^2(4a)^2(3b)^2(4b)^2(5a)^2(6a)^2(5b)^2(7a)^2(6b)^2(8a)^2(7b)^2(9a)^2(8b)^2$. The WBI value of this molecule for $C_{terminal(no\ attached\ hydrogen)}$-$C_{terminal(attached\ hydrogen)}$ = 1.07, $C_{central}$-$C_{terminal(no\ attached\ hydrogen)}$ = 1.18, and $C_{central}$-$C_{terminal(attached\ hydrogen)}$ = 0.77 represents all single bond character.

Again, in the case of spiro[2.2]pent-4-en-1-ylidene (**spiro-4**), the central atom is attached with a carbene carbon, two sp^2-hybridized carbon atom, and one sp^3-hybridized carbon atom. This molecule is 97 kcal mol^{-1} higher in energy than **1** and a minima on the C_5H_4 PES. The corresponding ptC structure is unstable with respect to isomerization process. The ground electronic state of this isomer is $^1A'$ (C_s molecular symmetry) with the electronic configuration $(1a')^2(1a'')^2(2\text{-}6a')^2(2a'')^2(7\text{-}9a')^2(3a'')^2(10\text{-}11a')^2(4a'')^2(12\text{-}13a')^2$. The WBI indices of **spiro-4** predict that C1-C2, C1-C3, C2-C3, C3-C4, and C3-C5 have a single bonding character, whereas C4-C5 bond possess a double bonding character.

3.4. Topological Analysis using AIM Theory

The presence of interatomic bonding interactions has been observed between the nuclei through careful analysis of the electron density distribution using topological methods. This is indicated by the existence of a (3, -1) critical point, and these interactions are characterized by their partial covalent behavior, as suggested by the negative $H(r_c)$ values in accordance with Bader's theory. According to this theory, interatomic states can be classified based on the magnitude of the Laplacian of the electron density, represented by $|V(r_c)|$. Bonds are classified as electrostatic if $|V(r_c)| < G(r_c)$, covalent if $|V(r_c)| > G(r_c)$, and partially covalent in the intermediate range of $G(r_c) < |V(r_c)| < 2G(r_c)$.

The AIM theory was used to investigate the electronic structure of pyramidal, spiro, and planar tetracoordinate geometries. The theory is based on the analysis of the electronic density distribution, $\rho(r_c)$, which provides much information such as the critical points related to bonds and rings and their respective eigenvalues and ellipticities. Another important analysis from the AIM theory is the Laplacian of the charge density, $\nabla^2 \rho(r_c)$, which is defined as the sum of the three principal curvatures of the function at each point of space. The density is locally concentrated in regions where $\nabla^2 \rho(r_c) < 0$ and $\rho(r_c)$ is a local maximum, and locally depleted in regions where $\nabla^2 \rho(r_c) > 0$ and $\rho(r_c)$ is a local minimum. In the molecular graph representing the pyramidane geometry (Figure 4), atoms are shown in violet, bond critical points in orange, and ring critical points in yellow. There are two types of bonds throughout the analysis: C-C bonds and C-H bonds. From the geometrical point of view, the **py-1** structure has 12 bond critical points, and the **py-2** structure has 11 bond critical points. This indicates all the bond paths. For **py-1**, index number 10, 11, and 12 correspond to bond critical points in 8(H)--4(C), 4(C)--1(C), and 4(C)--3(C), respectively. In contrast, in **py-2**, index number 10, 11, and 12 represent the same in 9(H)--2(C), 2(C)--4(C), and 2(C)--1(C) bonds, respectively. From the above table, the values of $H(r_c)$ and $|V(r_c)| > G(r_c)$ indicate that all the bonds are covalent in nature. Regarding

the planar tetracoordinate geometry, **ptC-1** contains the three distinct index numbers 10, 12, and 14 for the bonds 7(H)--5(C), 5(C)--3(C), and 5(C)--4(C), respectively. It shows all the possible bond critical points in the above figure. The same is true for **ptC-2**, where index numbers 10, 12, 13, 14, and 16 represent the bonds between 6(H)--5(C), 2(C)--1(C), 2(C)--3(C), 5(C)--3(C), and 5(C)--4(C), respectively. However, **ptC-3** shows eight bond critical points (BCPs), indicating that the initial structure is not stable and the ring is broken. The analysis of four plausible neutral geometries of spiro compounds revealed interesting results. AIM analysis showed that **spiro-1** and **spiro-4** both had 10 bond critical points. For **spiro-1**, index numbers 10, 11, and 12 were distinct and represented the bonds between 8(H)--2(C), 2(C)--3(C), and 2(C)--1(C), respectively. Similarly, for **spiro-4**, index numbers 10, 11, 13, 15, 16, and 18 were distinct and represented the bonds between 8(H)--4(C), 4(C)--5(C), 4(C)--3(C), 3(C)--2(C), 3(C)--1(C), and 2(C)--1(C), respectively. However, the geometries of **spiro-2** and **spiro-3** were found to be unstable. In the case of **spiro-2**, the three-membered ring towards the alkyne moiety was cleaved, resulting in a linear structure. Meanwhile, **spiro-3** had two three-membered rings that broke due to rupturing of the 1(C)--3(C) and 3(C)--5(C) bonds.

The stability of the ptC-containing molecules can be understood from the nature of the loan pairs located on the central carbon atom. The topology of the electron density provides a consistent mapping of the bonded and nonbonded electron pairs through analysis of the Laplacian of the electron density. One possibility to complement the nonempirical connectivity provided by the electron density is to use the electron localization function, ELF(r), proposed by Becke and Edgecombe [74]. The color-filled ELF plot in Figure 5 visually represents the degree of electron localization in a molecule, which is measured by the ELF value. This quantum chemical property ranges from 0 to 1, where 0 signifies a fully delocalized electron cloud and 1 signifies a fully localized electron cloud. The color gradients used in the plot highlights high electron density with bright red and low electron density with dark blue. This plot specifically demonstrates the significant localization between the C-H and C-C bonds of the molecule.

In accordance with the WBIs, the electron localization function (ELF) values in Table 3 (Column 10) suggest, for isomer **py-1** and **py-2,** the hydrogen atoms (H) bonded to the base carbon atoms (C) have a higher covalency than the C-C bonds between the apical positions. However, the covalency of all C-H bonds decreases going from **py-1** to **py-2**, while the covalency of C1-C3 and C1-C2 bonds increases going from **py-1** to **py-2**. The electron density between the C-C and C-H bonds is in the range of 0.69-0.99 (Table 3, column 6) indicating the strong localization of electrons. Similarly, the ELF analysis for the spiro compounds predicts that the covalency order for the C-H bonds is more comparable with the C-C bonds.

The bonding properties in three planar tetracoordinate geometries **ptC-1**, **ptC-2**, and **ptC-3** are discussed in detail in the following section. The ELF analysis of **ptC-1** predicts the covalency order as C5-H7 = C2-H9 = C4-H6 = C1-H8 > C5-C4 = C1-C2 > C3-C5 = C3-C2 = C2-C1 = C3-C4. It can be observed that the covalent bond between carbon and hydrogen atoms (C-H bond) is predominant over the bonds between carbon atoms (C-C bond). From the ELF analysis of **ptC-2**, the covalency order is found to be C5-H6 = C5-H7 = C4-H9 = C4-H8 > C1-C2 > C4-C5 > C3-C5 = C3-C4 > C2-C3 = C1-C3. Here, the covalency order of all the C-H bonds increase compared to **ptC-1**. Furthermore, the C4-C5 and C1-C2 bonds in **ptC-2** are less covalent than in **ptC-1**. However, they are more covalent than the C3-C4, C3-C5, C1-C3, and C2-C3 bonds but less covalent than the C-H bonds. In case of **ptC-3**, the ELF analysis predicts the covalency order as C5-H6 = C5-H7 = C1-H9 = C1-H8 > C4-C5 = C1-C2 > C4-C3 = C3-C2. The covalency of all C-H bonds decreases slightly compared to **ptC-2**. The C4-C5 and C1-C2 bonds are less covalent than in **ptC-2**, but they are more covalent than the C3-C4, C3-C5, C1-C3, and C2-C3 bonds. The covalency of the C2-C3 bond increases compared to **ptC-2**.

In summary, the covalency of the C-H bonds increases from **ptC-1** to **ptC-2**, then slightly decreases to **ptC-3**. The covalency of the C4-C5 and C1-C2 bonds decreases from

ptC-1 to **ptC-3**, then increases from **ptC-2** to **ptC-3**. The C3-C4 bond becomes more covalent from **ptC-1** to **ptC-3**, while the C2-C3 bond becomes less covalent from **ptC-1** to **ptC-2**. The C5-C3 and C1-C3 bonds decrease in covalency from **ptC-1** to **ptC-2**.

3.5. Structural Comparison between Different Spin States

We have extended our calculations to investigate the structural changes with respect to the change in the spin state of the molecules. Though the feasibility of different spin states cannot be explained through single reference theory, for brevity all the isomers have been geometrically optimized in their triplet spin state using DFT at the ωB97XD /6-3111+G(d,p) level of theory and the harmonic vibrational frequencies have been calculated. The singlet-triplet energy gaps for all the molecules have been listed in Table S4. We have found that the **ptC-1** is a fourth-order saddle point on the PES of C_5H_4 in its singlet spin state. However, the corresponding tetrahedral form, **spiro-1,** is a minimum energy structure. While analyzing the geometry in its triplet state, we observed that the central carbon of **ptC-1** is no longer in the same plane with the other four carbon atoms (Figure S3). The dihedral angle between any three-terminal carbon and the central carbon has become 11.90° and the positions of the hydrogen atoms have shifted downwards by 40° with respect to the plan of the four terminal carbon atoms. The triplet state of the **ptC-1** becomes a second-order saddle point. The singlet state is marginally stable compared to the triplet state ($\Delta E_{S\text{-}T}$ = 1.51 kcal mol^{-1}). Here we note that the corresponding tetrahedral form (**spiro-1**) becomes a third-order saddle point in the triplet spin state, having three negative vibrational frequencies. The optimized geometry of **ptC-1** in the quintet spin state is a minimum energy structure on the C_5H_4 PES, having no imaginary frequency at the same level of theory. However, the optimized structure in the quintet state converges more towards the pyramidane structure, as the hydrogen atoms are shifted downwards and the central carbon atom is being uplifted by 44.5° from the plane of the terminal carbon atoms.

The **ptC-2** is the only minimum isomer on the PES of C_5H_4, which possesses a planar tetracoordinate carbon in the singlet spin state. The molecule becomes a second-order saddle point in its triplet spin state. The positive singlet-triplet energy gap ($\Delta E_{S\text{-}T}$ = 60.69 kcal mol^{-1}) suggests the molecule is more stable in the singlet spin state. However, the **spiro-2** is a minimum structure. In the case of the **ptC-3** as well as the **spiro-3**, both isomerize to the more stable allene isomer (pent-1,2,3,4-tetraene) in their triplet electronic spin state.

3.6. Ab Initio Molecular Dynamics

The ab initio molecular dynamics simulations (AIMD) [68] have been carried out for all nine isomers at different temperatures to confirm their kinetic stability in their respective singlet ground electronic states. Atom-centered density matrix propagation (ADMP) is an extended Lagrangian molecular dynamics method which has been used to employ the atom-centered Gaussian basis functions and one-particle density matrix propagation. These simulations were executed in Gaussian 09 software at 1 atm pressure and temperatures of 10 K, 60 K, 120 K, and 29 8 K for 10,000 fs at the B3LYP/6-311+G(d,p) level of theory. The time evolution of the total energy of the minimum energy ptC isomer (**ptC-2**) at different temperatures is shown in Figure 5. AIMD results for other isomers at different temperatures are shown in the Supporting Information.

Again, most of the molecular geometry breaks at the room temperature (298 K). Figure 6 shows the energy oscillations and the geometrical changes of **ptC-2** happening within a 10,000 fs time scale at different temperatures (10 K, 60 K, 120 K, and 298 K). This analysis concludes that **ptC-2** is kinetically stable. Furthermore, most of the minimum energy isomers (**py-1**, **py-2**, **spiro-1**, **spiro-3**, and **spiro-4**) are kinetically stable at low temperatures (10 K, 60 K, and 120 K). Only **spiro-1** is kinetically stable at 298 K.

3.7. Aromatic Characteristics and Relative Stability of the Molecules

To gain a better understanding of these molecules, NICS values have been calculated. It is well known that NICS value provides the information about the aromaticity of the ring. The NICS(1Å) values for all molecules have been calculated at the B3LYP/6-311+G(d,p) level of theory and listed in Table 4. One ghost atom is placed in the center of the ring and another one is placed perpendicular to it at 1Å distance. The negative NICS value indicates the aromatic character present in the molecules whereas positive value corresponds to the antiaromatic character. All the molecules possess negative NICS(1Å) (except ptC-1 and spiro-2) which represent their aromatic characteristics. Pyramidane (py-1 and py-2) structures consist of two different type of rings (four-membered and three-membered rings). In case of py-1, both the rings are aromatic in nature (−9.14 ppm (four-membered ring); −10.43 ppm (three-membered ring)), whereas the four-membered ring (−4.72 ppm) of py-2 is less aromatic compared to the three-membered ring (−10.00 ppm). From the above observation, it can be clearly defined that py-1 is more aromatic than py-2, justifying more stability. This fact can be verified through the electron delocalization in the HOMO of both pyramidane structures. The HOMO of the py-1 is mainly delocalized in the apical carbon and the basal four-membered ring. In contrast, the HOMO of py-2 is mainly localized at the carbene carbon.

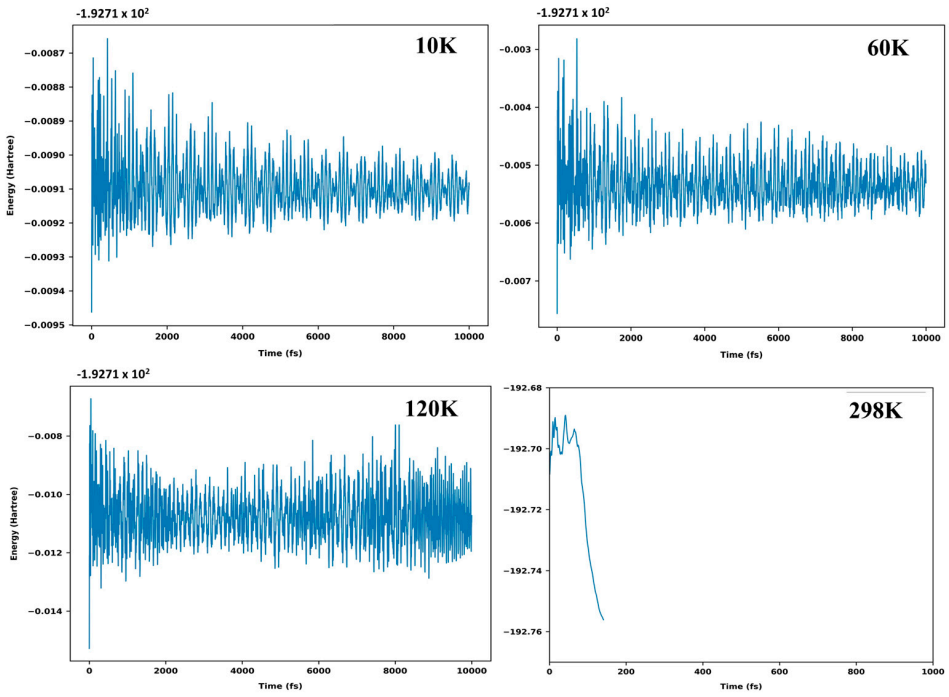

Figure 6. Energy evolution of isomer **ptC-2** ($^1A_1$) of C_5H_4 obtained from the AIMD simulation carried out at different temperatures (10 K, 60 K, 120 K, and 298 K) and 1 atm pressure for 10,000 fs at the B3LYP/6-311+G(d,p) level of theory.

The positive NICS value (11.20 ppm) of ptC-1 indicates its antiaromatic character. The HOMO picture reflects that the electrons are spread all over and the removal of the two electrons leads to the stabilization of the molecule by forming the two aromatic rings on both sides. The NICS value becomes −40.17 ppm, which specifies the high aromatic character of the system. For ptC-2, it was found that the NICS value is −18.87 ppm, which indicates the planar structure is aromatic in nature. It can be noted that in the HOMO, the electrons are delocalized mainly at the ethylene moiety, which stabilizes the molecule and widens the HOMO-LUMO energy gap. The electron delocalization can also be seen from the color-filled ELF graph where bright red colors indicate the same. This confirms the better stability and the reason to be a minimum on the C_5H_4 PES. The corresponding

tetrahedral form of ptC-2 (spiro-2) possesses a positive NICS value of 14.40 ppm, which is not a minimum energy isomer on the C_5H_4 PES. The NICS values for other spiro isomers are found to be negative, indicating the stability of the molecules.

Table 4. NICS(1Å) values (in ppm) for all the nine isomers calculated at B3LYP/6-311+G(d,p) level of theory. [a] represents the NICS value for the four-membered ring and [b] represents the value for the three-membered ring.

Molecules	NICS(1)
py-1	−9.14 [a]; −10.43 [b]
py-2	−4.72 [a]; −10.00 [b]
ptC-1	11.20
ptC-2	−18.87
ptC-3	−10.66
spiro-1	−5.38
spiro-2	14.40
spiro-3	−11.82
spiro-4	−14.02

4. Conclusions

For many years, researchers have been searching for the planar tetracoordinated carbon atoms as a minimum on various potential energy surfaces. Though the neutral form of **ptC-1** is a fourth-order saddle point, the dication form is a minimum on the PES of C_5H_4 as it gains the aromatic character by forming the two cyclopropenyl rings. Among the three ptCs, the **ptC-2** has been found to be a minimum on the PES of C_5H_4. It is energetically 14 kcal mol^{-1} more stable than the corresponding tetrahedral form (**spiro-2**). The electron distributions of HOMO and the negative NICS value indicate the greater stability of the **ptC-2** molecule and its aromatic nature. On the other hand, **spiro-2** has a positive NICS value reflecting its antiaromatic nature. The significant HOMO-LUMO energy gap of **ptC-2** ($\Delta E_{HOMO\text{-}LUMO}$ = 9.04 eV), compared to **spiro-2** ($\Delta E_{HOMO\text{-}LUMO}$ = 6.89 eV), might correlate to the higher stability of the planar form. In addition, the high dipole moment value (μ = 4.64 D) of **ptC-2** might help to detect this molecule in ISM or in laboratory. The **ptC-3** (a transition state) connects the stereomutation of **spiro-3.** The **spiro-1**, **spiro-3**, and **spiro-4** are minima on the C_5H_4 PES but the **spiro-2** is a second-order saddle point. The WBIs and the topological analysis of AIM calculations reveal the bond order and the bonding patterns between different C-C and C-H bonds. Along with this, AIMD calculations have been performed at different temperatures. This study reveals that all the molecules are kinetically unstable at 298 K except **spiro-1,** but the stationary points that are minima are stable at low temperature (10 K, 60 K, 120 K) conditions. It can be concluded that these molecules may be unstable in room temperature but stable in the exotic conditions like the interstellar medium.

Supplementary Materials: The following supporting information can be downloaded at: https://www.mdpi.com/article/10.3390/atoms11060096/s1, Figure S1: Possible 2D structure of initial guess isomers; Figure S2: Optimized geometries of all nine isomers in their triplet spin state calculated at the B3LYP/6-311+G(d,p) level of theory; Figure S3: Energy profile and the structural changes of **ptC-1** with respect to the change in spin state with the ground state molecular term symbol and number of imaginary frequencies; Figure S4: Intrinsic Reaction Coordinate (IRC) for the transition state **ptC-3** calculated at B3LYP/6-311+G(d,p) level of theory; Figure S5: Energy evolution of isomer **py-1** ($^1A_1$) of C_5H_4 obtained from the AIMD simulation carried out at different temperature (10K, 60 K and 120 K) and 1 atm pressure for 10,000 fs at the B3LYP/6-311+G(d,p) level of theory; Figure S6: Energy evolution of isomer **py-2** ($^1A'$) of C_5H_4 obtained from the AIMD simulation carried out at different temperature (10 K, 60 K and 120 K) and 1 atm pressure for 10,000 fs at the B3LYP/6-311+G(d,p) level of theory; Figure S7: Energy evolution of isomer **spiro-1** (^1E) of C_5H_4 obtained from the AIMD simulation carried out at different temperature (10 K, 60 K, and 298 K) and 1 atm pressure for 10,000 fs at the B3LYP/6-311+G(d,p) level of theory; Figure S8: Energy evolution of isomer **spiro-3** (^1B) of C_5H_4

obtained from the AIMD simulation carried out at different temperature (10 K, 60 K and 120 K) and 1 atm pressure for 10,000 fs at the B3LYP/6-311+G(d,p) level of theory; Figure S9: Energy evolution of isomer **spiro-4** ($^1A'$) of C_5H_4 obtained from the AIMD simulation carried out at different temperature (10 K, 60 K and 120 K) and 1 atm pressure for 10,000 fs at the B3LYP/6-311+G(d,p) level of theory; Table S1: Optimized geometries of the C_5H_4 isomers in singlet ground electronic state in Cartesian coordinates (in Angstrom units) obtained at CCSD(T)/cc-pVTZ level of theory; Table S2: Optimized geometries of the C_5H_4 isomers in triplet ground electronic state and quintet electronic state of **ptC-1** in Cartesian coordinates (in Angstrom units) obtained at B3LYP/6-311+G(d,p) level of theory; Table S3: Dipole moments in different axis (in Debye), total dipole moment (in Debye), Centrifugal distortion constants, and rotational constants (in MHz) of C_5H_4 isomers in their ground electronic states calculated at the CCSD(T)/cc-pVTZ level of theory; Table S4: The energy gap between singlet and triplet spin state of all nine isomers of C_5H_4 at B3LYP/6-311+G(d,p) level of theory; Table S5: The energy gap between singlet and triplet spin state (ΔE_{st} in kcal mol^{-1}), number of imaginary frequencies (NImag), and dipole moment ($|\mu|$ in Debye) of all nine isomers of C_5H_4 at ωB97XD/6-311+G(d,p) level of theory; Table S6: Electron density descriptors (in a.u.) at the (3, –1) bond critical points (BCP) obtained from the B3LYP/6-311+G(d,p) level for all the nine isomers. The topological parameters such as Hamiltonian Kinetic Energy $K(r_c)$, $\rho(r_c)$, Laplacian Electron Density ($\nabla^2\rho(r_c)$), Lagrangian Kinetic Energy $G(r_c)$, Potential Energy Density $V(r_c)$, Energy Density $E(r_c)$ or $H(r_c)$, ELF, $G(r_c)/V(r_c)$, and $G(r_c)/\rho(r_c)$ at the critical points are also given; Table S7: WBI Indices for all nine isomers calculated at B3LYP/6-311+G(d,p) level of theory.

Author Contributions: Conceptualization, S.G. (Subhas Ghosal); methodology, A.A., V.S.T. and S.G. (Subhas Ghosal); software, S.S., T.R. and S.G. (Sandip Giri); validation, S.G. (Subhas Ghosal), V.S.T. and A.A.; formal analysis, S.S., T.R. and S.G. (Sandip Giri); investigation, S.S., T.R. and S.G. (Sandip Giri); resources, S.G. (Subhas Ghosal), A.A. and V.S.T.; data curation, S.S., T.R. and S.G. (Sandip Giri); writing—original draft preparation, S.S., T.R., S.G. (Sandip Giri) and S.G. (Subhas Ghosal); writing—review and editing, S.G. (Subhas Ghosal), A.A. and V.S.T.; visualization, S.S., T.R., S.G. (Subhas Ghosal), A.A. and V.S.T.; supervision, S.G. (Subhas Ghosal), A.A. and V.S.T.; project administration, S.G. (Subhas Ghosal), A.A. and V.S.T. All authors have read and agreed to the published version of the manuscript.

Funding: S.G. and A.A. thanks Govt. of India (GoI) for grant No. DST/NSM/R&D_HPC_Applications/2021/21 for the Paramshakti HPC facilities at IIT Kharagpur. S.G. thanks for the computational facilities in NITD supported by EMR/2017/002653 and V.S.T. thanks U.S. Department of Defense for DURIP grant W911NF-10-1-0157 and NSF CRIF grant CHE-0947087 at SDSU.

Data Availability Statement: Data available in the article or Supplementary Materials.

Acknowledgments: Subhas Ghosal and Anakuthil Anoop thanks Govt. of India (GoI) for grant no. DST/NSM/R&D_HPC_Applications/2021/21 for the Paramshakti HPC facilities at IIT Kharagpur and the doctoral fellowship for Sayon Satpati Computational facilities in NITD supported by EMR/2017/002653. Support provided at SDSU (for Venkatesan S. Thimmakondu) by DURIP grant W911NF-10-1-0157 from the U.S. Department of Defense and NSF CRIF grant CHE-0947087 are gratefully acknowledged. Tarun Roy thanks NITD for the doctoral fellowship. Sandip Giri thanks IITKGP for the doctoral fellowship.

Conflicts of Interest: The authors declare no conflict of interest.

References

1. van't Hoff, J.H. A suggestion looking to the extension into space of the structural formulas at present used in chemistry, and a note upon the relation between the optical activity and the chemical constitution of organic compounds. *Arch. Neerl. Sci. Exactes Nat.* **1874**, *9*, 445–454.
2. Le Bel, J.A. Sur les relations qui existent entre les formules atomiques des corps organiques et le pouvoir rotatoire de leurs dissolutions. *Bull. Soc. Chim. Fr.* **1874**, *22*, 337–347.
3. Minkin, V.I.; Minyaev, R.M.; Hoffmann, R. Non-classical structures of organic compounds: Unusual stereochemistry and hypercoordination. *Russ. Chem. Rev.* **2002**, *71*, 869–892. [CrossRef]
4. Vassilev-Galindo, V.; Pan, S.; Donald, K.J.; Merino, G. Planar pentacoordinate carbons. *Nat. Rev. Chem.* **2018**, *2*, 0114. [CrossRef]
5. Yang, L.M.; Ganz, E.; Chen, Z.; Wang, Z.X.; Schleyer, P.V.R. Four decades of the chemistry of planar hypercoordinate compounds. *Angew. Chem. Int. Ed.* **2015**, *54*, 9468–9501. [CrossRef] [PubMed]

6. Shan, C.; Dong, S.; Yao, S.; Zhu, J.; Driess, M. Synthesis and Reactivity of an Anti-van't Hoff/Le Bel Compound with a Planar Tetracoordinate Silicon(II) Atom. *J. Am. Chem. Soc.* **2023**, *145*, 7084–7089. [CrossRef] [PubMed]
7. Liu, S.; Xia, D.; Baumgarten, M. Rigidly Fused Spiro-Conjugated π-Systems. *ChemPlusChem* **2021**, *86*, 36–48.
8. Randić, M.; Rubčić, A.; Klasinc, L. Hybridization in highly strained small ring hydrocarbons—III: Unsaturated spiro-compounds. *Tetrahedron* **1971**, *27*, 5771–5777. [CrossRef]
9. Delouche, T.; Hissler, M.; Bouit, P.-A. Polycyclic aromatic hydrocarbons containing heavy group 14 elements: From synthetic challenges to optoelectronic devices. *Coord. Chem. Rev.* **2022**, *464*, 214553. [CrossRef]
10. Firme, C.L. Cycloalkanes, Bicyclic, and Caged Hydrocarbons. In *Introductory Organic Chemistry and Hydrocarbons*; CRC Press: Boca Raton, FL, USA, 2019; pp. 241–266.
11. Leyva-Parra, L.; Inostroza, D.; Yañez, O.; Cruz, J.C.; Garza, J.; García, V.; Tiznado, W. Persistent planar tetracoordinate carbon in global minima structures of silicon-carbon clusters. *Atoms* **2022**, *10*, 27. [CrossRef]
12. Pancharatna, P.D.; Méndez-Rojas, M.A.; Merino, G.; Vela, A.; Hoffmann, R. Planar tetracoordinate carbon in extended systems. *J. Am. Chem. Soc.* **2004**, *126*, 15309–15315. [CrossRef] [PubMed]
13. Thirumoorthy, K.; Thimmakondu, V.S. Flat crown ethers with planar tetracoordinate carbon atoms. *Int. J. Quantum. Chem.* **2021**, *121*, e26479. [CrossRef]
14. Thirumoorthy, K.; Karton, A.; Thimmakondu, V.S. From High-Energy C7H2 Isomers with A Planar Tetracoordinate Carbon Atom to An Experimentally Known Carbene. *J. Phys. Chem. A* **2018**, *122*, 9054–9064. [CrossRef] [PubMed]
15. Wang, L.-S.; Boldyrev, A.I.; Li, X.; Simons, J. Experimental Observation of Pentaatomic Tetracoordinate Planar Carbon-Containing Molecules. *J. Am. Chem. Soc.* **2000**, *122*, 7681–7687. [CrossRef]
16. Xu, J.; Zhang, X.; Yu, S.; Ding, Y.-H.; Bowen, K.H. Identifying the Hydrogenated Planar Tetracoordinate Carbon: A Combined Experimental and Theoretical Study of CAl4H and $CAl4H^-$. *J. Phys. Chem. Lett.* **2017**, *8*, 2263–2267. [CrossRef]
17. Röttger, D.; Erker, G. Compounds Containing Planar-Tetracoordinate Carbon. *Angew. Chem. Int. Ed.* **1997**, *36*, 812–827. [CrossRef]
18. Hoffmann, R.; Alder, R.W.; Wilcox, C.F., Jr. Planar tetracoordinate carbon. *J. Am. Chem. Soc.* **1970**, *92*, 4992–4993. [CrossRef]
19. McGrath, M.P.; Radom, L. Alkaplanes: A Class of Neutral Hydrocarbons Containing a Potentially Planar Tetracoordinate Carbon. *J. Am. Chem. Soc.* **1993**, *115*, 3320–3321. [CrossRef]
20. Wang, Z.-X.; Schleyer, P.v.R. The theoretical design of neutral planar tetracoordinate carbon molecules with C (C) 4 substructures. *J. Am. Chem. Soc.* **2002**, *124*, 11979–11982. [CrossRef]
21. Wang, Z.-X.; Schleyer, P.v.R. A new strategy to achieve perfectly planar carbon tetracoordination. *J. Am. Chem. Soc.* **2001**, *123*, 994–995. [CrossRef]
22. Sorger, K.; Ragué; Schleyer, P.V. Planar and inherently non-tetrahedral tetracoordinate carbon: A status report. *J. Mol. Struct.* **1995**, *338*, 317–346. [CrossRef]
23. Siebert, W.; Gunale, A. Compounds containing a planar-tetracoordinate carbon atom as analogues of planar methane. *Chem. Soc. Rev.* **1999**, *28*, 367–371. [CrossRef]
24. Rasmussen, D.R.; Radom, L. Planar-Tetracoordinate Carbon in a Neutral Saturated Hydrocarbon: Theoretical Design and Characterization. *Angew. Chem. Int. Ed.* **1999**, *38*, 2875–2878. [CrossRef]
25. Das, P.; Khatun, M.; Anoop, A.; Chattaraj, P.K. CSinGe4−n2+ (n = 1–3): Prospective systems containing planar tetracoordinate carbon (ptC). *Phys. Chem. Chem. Phys.* **2022**, *24*, 16701–16711. [CrossRef] [PubMed]
26. Wang, Z.X.; Von Ragué Schleyer, P. Construction principles of "Hyparenes": Families of molecules with planar pentacoordinate carbons. *Science* **2001**, *292*, 2465–2469. [CrossRef]
27. Yañez, O.; Vásquez-Espinal, A.; Báez-Grez, R.; Rabanal-León, W.A.; Osorio, E.; Ruiz, L.; Tiznado, W. Carbon rings decorated with group 14 elements: New aromatic clusters containing planar tetracoordinate carbon. *N. J. Chem.* **2019**, *43*, 6781–6785. [CrossRef]
28. Wang, M.-H.; Orozco-Ic, M.; Leyva-Parra, L.; Tiznado, W.; Barroso, J.; Ding, Y.-H.; Cui, Z.-H.; Merino, G. Planar Tetracoordinate Carbons in Allene-Type Structures. *J. Phys. Chem. A* **2021**, *125*, 3009–3014. [CrossRef] [PubMed]
29. Job, N.; Khatun, M.; Thirumoorthy, K.; CH, S.S.R.; Chandrasekaran, V.; Anoop, A.; Thimmakondu, V.S. CAl4Mg0/−: Global Minima with a Planar Tetracoordinate Carbon Atom. *Atoms* **2021**, *9*, 24. [CrossRef]
30. Sateesh, B.; Srinivas Reddy, A.; Narahari Sastry, G. Towards design of the smallest planar tetracoordinate carbon and boron systems. *J. Comput. Chem.* **2007**, *28*, 335–343. [CrossRef]
31. Suresh, C.H.; Frenking, G. Direct 1−3 Metal−Carbon Bonding and Planar Tetracoordinated Carbon in Group 6 Metallacyclobutadienes. *Organometallics* **2010**, *29*, 4766–4769. [CrossRef]
32. Thirumoorthy, K.; Chandrasekaran, V.; Cooksy, A.L.; Thimmakondu, V.S. Kinetic Stability of $Si_2C_5H_2$ Isomer with a Planar Tetracoordinate Carbon Atom. *Chemistry* **2020**, *3*, 13–27. [CrossRef]
33. Rasmussen, D.R.; Radom, L. Hemispiroalkaplanes: Hydrocarbon Cage Systems with a Pyramidal-Tetracoordinate Carbon Atom and Remarkable Basicity. *Chem. Eur. J.* **2000**, *6*, 2470–2483. [CrossRef] [PubMed]
34. Priyakumar, U.D.; Reddy, A.S.; Sastry, G.N. The design of molecules containing planar tetracoordinate carbon. *Tetrahedron Lett.* **2004**, *45*, 2495–2498. [CrossRef]
35. Karton, A.; Thimmakondu, V.S. From Molecules with a Planar Tetracoordinate Carbon to an Astronomically Known C_5H_2 Carbene. *J. Phys. Chem. A* **2022**, *126*, 2561–2568. [CrossRef]
36. Cabezas, C.; Tercero, B.; Agúndez, M.; Marcelino, N.; Pardo, J.; de Vicente, P.; Cernicharo, J. Cumulene carbenes in TMC-1: Astronomical discovery of l-H_2C_5. *Astron. Astrophys.* **2021**, *650*, L9. [CrossRef]

37. Cernicharo, J.; Agúndez, M.; Cabezas, C.; Tercero, B.; Marcelino, N.; Pardo, J.R.; de Vicente, P. Pure hydrocarbon cycles in TMC-1: Discovery of ethynyl cyclopropenylidene, cyclopentadiene, and indene. *Astron. Astrophys.* **2021**, *649*, L15. [CrossRef]
38. Blanksby, S.J.; Dua, S.; Bowie, J.H.; Schröder, D.; Schwarz, H. Gas-phase syntheses of three isomeric C_5H_2 radical anions and their elusive neutrals. a joint experimental and theoretical study. *J. Phys. Chem. A* **1998**, *102*, 9949–9956. [CrossRef]
39. He, C.; Galimova, G.R.; Luo, Y.; Zhao, L.; Eckhardt, A.K.; Sun, R.; Mebel, A.M.; Kaiser, R.I. A chemical dynamics study on the gas-phase formation of triplet and singlet C_5H_2 carbenes. *Proc. Natl. Acad. Sci. USA* **2020**, *117*, 30142–30150. [CrossRef]
40. Sun, Y.-L.; Huang, W.-J.; Lee, S.-H. Formation of C_3H_2, C_5H_2, C_7H_2, and C_9H_2 from reactions of CH, C_3H, C_5H, and C_7H radicals with C_2H_2. *Phys. Chem. Chem. Phys.* **2016**, *18*, 2120–2129. [CrossRef]
41. Jayakumari, C.M.; Nag, P.; Isukapalli, S.V.K.; Vennapusa, S.R. Exploring the Excited-State Nonadiabatic Effects in the Semisaturated Planar Tetracoordinated Carbon Molecule C_7H_4. *Atoms* **2022**, *10*, 10. [CrossRef]
42. Yadav, K.; Lourderaj, U.; Priyakumar, U.D. Stereomutation in Tetracoordinate Centers via Stabilization of Planar Tetracoordinated Systems. *Atoms* **2021**, *9*, 79. [CrossRef]
43. Stohrer, W.D.; Hoffmann, R. Bond-stretch isomerism and polytopal rearrangements in (CH)5+, (CH)5−, and (CH)4CO. *J. Am. Chem. Soc.* **1972**, *94*, 1661–1668. [CrossRef]
44. Minkin, V.; Zefirov, N.; Korobov, M.; Averina, N.; Boganov, A.; Nivorozhkin, L. 1,3,5-Trimethyl Derivative of the Square Pyramidal Cation (Ch) 5+. *Chem. Inf. Dienst.* **1981**, *12*, 2616–2618.
45. Krogh-Jespersen, K.; Chandrasekhar, J.; Schleyer, P.V.R. Geometries and relative energies of some $C_6H_5^+$ and $C_5H_5Si^+$ isomers. Pyramidal (nido) vs. planar, cyclic structures. *J. Org. Chem.* **1980**, *45*, 1608–1614. [CrossRef]
46. Kenny, J.P.; Krueger, K.M.; Rienstra-Kiracofe, J.C.; Schaefer, H.F. C_5H_4: Pyramidane and its low-lying isomers. *J. Phys. Chem. A* **2001**, *105*, 7745–7750. [CrossRef]
47. Lee, V.Y.; Gapurenko, O.A.; Ito, Y.; Meguro, T.; Sugasawa, H.; Sekiguchi, A.; Minyaev, R.M.; Minkin, V.I.; Herber, R.H.; Gornitzka, H. Pyramidanes: The Covalent Form of the Ionic Compounds. *Organometallics* **2016**, *35*, 346–356. [CrossRef]
48. Gapurenko, O.A.; Minyaev, R.M.; Minkin, V.I. Silicon analogues of pyramidane: A quantum-chemical study. *Mendeleev. Commun.* **2012**, *22*, 8–10. [CrossRef]
49. Moreno-Armenta, M.G.; Pearce, H.R.; Winter, P.; Cooksy, A.L. Computational search for metastable high-spin C_5Hn (n = 4, 5, 6) species. *Comput. Theor. Chem.* **2018**, *1140*, 1–6. [CrossRef]
50. Adewale, R.; da Silva, G. Kinetics of C_5H_4 isomer + H reactions and incorporation of C_5Hx (x = 3–5) chemistry into a detailed chemical kinetic model. *Combust. Flame* **2021**, *227*, 227–237. [CrossRef]
51. Lee, C.; Yang, W.; Parr, R.G. Development of the Colle-Salvetti correlation-energy formula into a functional of the electron density. *Phys. Rev. B* **1988**, *37*, 785. [CrossRef]
52. Becke, A.D. Density-functional exchange-energy approximation with correct asymptotic behavior. *Phys. Rev. A* **1988**, *38*, 3098. [CrossRef] [PubMed]
53. Krishnan, R.; Binkley, J.S.; Seeger, R.; Pople, J.A. Self-consistent molecular orbital methods. XX. A basis set for correlated wave functions. *J. Chem. Phys.* **1980**, *72*, 650–654. [CrossRef]
54. Clark, T.; Chandrasekhar, J.; Spitznagel, G.W.; Schleyer, P.V.R. Efficient diffuse function-augmented basis sets for anion calculations. III. The 3-21+ G basis set for first-row elements, Li–F. *J. Comput. Chem.* **1983**, *4*, 294–301. [CrossRef]
55. Frisch, M.J.; Head-Gordon, M.; Pople, J.A. A direct MP2 gradient method. *Chem. Phys. Lett.* **1990**, *166*, 275–280. [CrossRef]
56. Grimme, S.; Antony, J.; Ehrlich, S.; Krieg, H. A consistent and accurate ab initio parametrization of density functional dispersion correction (DFT-D) for the 94 elements H-Pu. *J. Chem. Phys.* **2010**, *132*, 154104. [CrossRef]
57. Chai, J.-D.; Head-Gordon, M. Long-range corrected hybrid density functionals with damped atom–atom dispersion corrections. *Phys. Chem. Chem. Phys.* **2008**, *10*, 6615–6620. [CrossRef]
58. Bartlett, R.J.; Purvis, G.D. Many-body perturbation theory, coupled-pair many-electron theory, and the importance of quadruple excitations for the correlation problem. *Int. J. Quantum. Chem.* **1978**, *14*, 561–581. [CrossRef]
59. Pople, J.; Krishnan, R.; Schlegel, H.; Binkley, J. Electron correlation theories and their application to the study of simple reaction potential surfaces. *Int. J. Quantum. Chem.* **1978**, *14*, 545–560. [CrossRef]
60. Raghavachari, K.; Trucks, G.W.; Pople, J.A.; Head-Gordon, M. A fifth-order perturbation comparison of electron correlation theories. *Chem. Phys. Lett.* **1989**, *157*, 479–483. [CrossRef]
61. Peterson, K.A.; Dunning, T.H., Jr. Accurate correlation consistent basis sets for molecular core–valence correlation effects: The second row atoms Al–Ar, and the first row atoms B–Ne revisited. *J. Chem. Phys.* **2002**, *117*, 10548–10560. [CrossRef]
62. Kendall, R.A.; Dunning, T.H., Jr.; Harrison, R.J. Electron affinities of the first-row atoms revisited. Systematic basis sets and wave functions. *J. Chem. Phys.* **1992**, *96*, 6796–6806. [CrossRef]
63. Woon, D.E.; Dunning, T.H., Jr. Gaussian basis sets for use in correlated molecular calculations. V. Core-valence basis sets for boron through neon. *J. Chem. Phys.* **1995**, *103*, 4572–4585. [CrossRef]
64. Frisch, M.J.; Schlegel, H.B.; Scuseria, G.E.; Robb, M.A.; Cheeseman, J.R.; Scalmani, G.; Barone, V.; Mennucci, B.; Petersson, G.A.; Nakatsuji, H.; et al. *Gaussian 09, Revision D.01*; Gaussian, Inc.: Wallingford, CT, USA, 2013.
65. Matthews, D.A.; Cheng, L.; Harding, M.E.; Lipparini, F.; Stopkowicz, S.; Jagau, T.-C.; Szalay, P.G.; Gauss, J.; Stanton, J.F. Coupled-cluster techniques for computational chemistry: The CFOUR program package. *J. Chem. Phys.* **2020**, *152*, 214108. [CrossRef] [PubMed]
66. Neese, F. Software update: The ORCA program system, version 4.0. *Comput. Mol. Sci.* **2018**, *8*, e1327. [CrossRef]

67. Lu, T.; Chen, F. Multiwfn: A multifunctional wavefunction analyzer. *J. Comput. Chem.* **2012**, *33*, 580–592. [CrossRef] [PubMed]
68. Schlegel, H.B.; Millam, J.M.; Iyengar, S.S.; Voth, G.A.; Daniels, A.D.; Scuseria, G.E.; Frisch, M.J. Ab initio molecular dynamics: Propagating the density matrix with Gaussian orbitals. *J. Chem. Phys.* **2001**, *114*, 9758–9763. [CrossRef]
69. Walmsley, C.M.; Jewell, P.R.; Snyder, L.E.; Winnewisser, G. Detection of interstellar methyldiacetylene (CH_3C_4H) in dark dust cloud TMC1. *Astron. Astrophys.* **1984**, *134*, L11–L14.
70. MacLeod, J.M.; Avery, L.W.; Broten, N.W. The detection of interstellar methyldiacetylene (CH_3C_4H). *Astrophys. J.* **1984**, *282*, L89–L92. [CrossRef]
71. Araki, M.; Takano, S.; Sakai, N.; Yamamoto, S.; Oyama, T.; Kuze, N.; Tsukiyama, K. Long Carbon Chains in the Warm Carbon-chain-chemistry Source L1527: First Detection of C_7H in Molecular Clouds. *Astrophys. J.* **2017**, *847*, 51. [CrossRef]
72. Cabezas, C.; Fuentetaja, R.; Roueff, E.; Agúndez, M.; Tercero, B.; Marcelino, N.; Pardo, J.R.; de Vicente, P.; Cernicharo, J. New deuterated species in TMC-1: Detection of CH_2DC_4H with the QUIJOTE line survey. *Astron. Astrophys.* **2022**, *657*, L5. [CrossRef]
73. Tsuneda, T.; Song, J.-W.; Suzuki, S.; Hirao, K. On Koopmans' theorem in density functional theory. *J. Chem. Phys.* **2010**, *133*, 174101. [CrossRef] [PubMed]
74. Merino, G.; Méndez-Rojas, M.A.; Beltrán, H.I.; Corminboeuf, C.; Heine, T.; Vela, A. Theoretical Analysis of the Smallest Carbon Cluster Containing a Planar Tetracoordinate Carbon. *J. Am. Chem. Soc.* **2004**, *126*, 16160–16169. [CrossRef] [PubMed]